Peptidomimetic-based identification of FDA approved compounds inhibiting IRE1 activity

Dimitrios Doultsinos, Antonio Carlesso, Chetan Chintha, James C Paton, Adrienne W Paton, Afshin Samali, Eric Chevet, Leif A Eriksson

▶ **To cite this version:**

Dimitrios Doultsinos, Antonio Carlesso, Chetan Chintha, James C Paton, Adrienne W Paton, et al.. Peptidomimetic-based identification of FDA approved compounds inhibiting IRE1 activity. FEBS Journal, 2021, 288 (3), pp.945-960. 10.1111/febs.15372 . hal-02862262

HAL Id: hal-02862262

https://univ-rennes.hal.science/hal-02862262

Submitted on 23 Jan 2023

HAL is a multi-disciplinary open access archive for the deposit and dissemination of scientific research documents, whether they are published or not. The documents may come from teaching and research institutions in France or abroad, or from public or private research centers.

L'archive ouverte pluridisciplinaire **HAL**, est destinée au dépôt et à la diffusion de documents scientifiques de niveau recherche, publiés ou non, émanant des établissements d'enseignement et de recherche français ou étrangers, des laboratoires publics ou privés.

Distributed under a Creative Commons Attribution 4.0 International License

Check for updates

The FEBS Journal

FEBS PRESS science publishing by scientists

Peptidomimetic-based identification of FDA-approved compounds inhibiting IRE1 activity

Dimitrios Doultsinos[1,2], Antonio Carlesso[3], Chetan Chintha[4], James C. Paton[5], Adrienne W. Paton[5], Afshin Samali[4], Eric Chevet[1,2] and Leif A. Eriksson[3]

1 Proteostasis & Cancer Team INSERM U1242 'Chemistry, Oncogenesis Stress Signaling', Université de Rennes, France
2 Centre de Lutte contre le Cancer Eugène Marquis, Rennes, France
3 Department of Chemistry and Molecular Biology, University of Gothenburg, Sweden
4 Apoptosis Research Centre, School of Natural Sciences, NUI Galway, Ireland
5 Research Centre for Infectious Diseases, Department of Molecular and Biomedical Science, University of Adelaide, SA, Australia

Keywords
endoplasmic reticulum; glioblastoma; inhibitors; IRE1; unfolded protein response

Correspondence
E. Chevet, Proteostasis & Cancer Team INSERM U1242 'Chemistry, Oncogenesis Stress Signaling', Université de Rennes, Rennes, France
Tel: +33 (0)223237258
E-mail: eric.chevet@inserm.fr
L. A. Eriksson, Department of Chemistry and Molecular Biology, University of Gothenburg, Göteborg, Sweden
Tel: +46 (0)317869117
E-mail: leif.eriksson@chem.gu.se

(Received 19 December 2019, revised 6 April 2020, accepted 19 May 2020)

doi:10.1111/febs.15372

Inositol-requiring enzyme 1 (IRE1) is a bifunctional serine/threonine kinase and endoribonuclease that is a major mediator of the unfolded protein response (UPR) during endoplasmic reticulum (ER) stress. Tumour cells experience ER stress due to adverse environmental cues such as hypoxia or nutrient shortage and high metabolic/protein-folding demand. To cope with those stresses, cancer cells utilise IRE1 signalling as an adaptive mechanism. Here, we report the discovery of the FDA-approved compounds methotrexate, cefoperazone, folinic acid and fludarabine phosphate as IRE1 inhibitors. These were identified through a structural exploration of the IRE1 kinase domain using IRE1 peptide fragment docking and further optimisation and pharmacophore development. The inhibitors were verified to have an impact on IRE1 activity *in vitro* and were tested for their ability to sensitise human cell models of glioblastoma multiforme (GBM) to chemotherapy. We show that all molecules identified sensitise glioblastoma cells to the standard-of-care chemotherapy temozolomide (TMZ).

Introduction

The unfolded protein response (UPR) is a homeostatic mechanism designed to alleviate endoplasmic reticulum (ER) stress caused by the accumulation of misfolded proteins. The UPR senses accumulation of misfolded proteins through foldases such as protein disulfide isomerases (PDI4-6) and chaperones (BiP) and carries

Abbreviations
AACR, American Association for Cancer Research; ANOVA, analysis of variance; ATCC, American Type Culture Collection; ATF6, activating transcription factor 6; ATP, adenosine triphosphate; BiP, binding immunoglobulin protein; DMEM, Dulbecco's modified Eagle's medium; DMSO, dimethyl sulfoxide; DTT, dithiothreitol; *E. coli*, *Escherichia coli*; ER, endosplasmic reticulum; FDA, Food and Drug Administration; GBM, glioblastoma multiforme; IRE1, inositol-requiring enzyme 1; KIRA, kinase-inhibiting RNase attenuator; MOE, molecular operating environment; MST, microscale thermophoresis; MYC, master regulator of cell cycle entry; NTA, nanoparticle tracking analysis; OPLS, optimised potential for liquid simulations; PBS, phosphate-buffered saline; PBST, phosphate-buffered saline with Tween; PDB, Protein Data Bank; PDI, protein disulfide isomerase; PDX, patient-derived xenograft; PERK, protein kinase RNA-like endoplasmic reticulum kinase; PVDF, polyvinylidene difluoride; RIPA, radioimmunoprecipitation assay buffer; SD, standard deviation; SDS/PAGE, sodium dodecyl sulfate/polyacrylamide gel; SP, single precision; SubAB, subtilase cytotoxin; TMZ, temozolomide; TNBC, triple-negative breast cancer; Tun, tunicamycin; U87MG, Uppsala 87 Malignant Glioma; UPR, unfolded protein response; WST1, water-soluble tetrazolium salts; XBP1, X-box binding protein 1; XBP1s, spliced form of X-box binding protein 1; XP, extra precision.

This is an open access article under the terms of the Creative Commons Attribution License, which permits use, distribution and reproduction in any medium, provided the original work is properly cited.

17424658, 2021, 3, Downloaded from https://febs.onlinelibrary.wiley.com/doi/10.1111/febs.15372 by Universite de Rennes, Wiley Online Library on [23/01/2023]. See the Terms and Conditions (https://onlinelibrary.wiley.com/terms-and-conditions) on Wiley Online Library for rules of use; OA articles are governed by the applicable Creative Commons License

out its effects on protein quality control, translation attenuation and protein clearance through three main transducers: ATF6, PERK and the most evolutionarily conserved IRE1 [1]. Sustained stress would programme most physiologically normal cells for apoptosis; however, cancer cells utilise a hyperadaptive UPR to survive an environment composed of hypoxia, low pH and nutrient deprivation on top of therapeutic insults [2]. It has been shown that IRE1 in particular plays a decisive role in tumorigenesis and tumour aggressiveness, as well as post-therapy response in, for example, cancers of the breast, pancreas, prostate and brain [3–6]. This pertains to the possibility that targeting IRE1 activity could lead to sensitisation of tumours to current therapies as cancer cells would exhibit reduced capacity to cope with the hostile environment. Indeed, such studies have been performed in triple-negative breast cancer (TNBC) showing that the inhibition of IRE1 RNase activity with salicylaldehyde MKC8866 increased paclitaxel-dependent attenuation of TNBC development in mouse xenograft models [7] or in glioblastoma multiforme (GBM) models [8]. Further to this, MKC8866 treatment greatly enhanced the efficacy of docetaxel in regressing MYC-overexpressing tumours in breast cancer PDX models [9]. This covalent inhibitor is currently tested on other types of cancers.

IRE1 activity inhibition can be mediated by compounds targeting either the ATP-binding kinase domain or directly the RNase domain. Direct RNase pharmacological inhibitors include 4μ8c, STF-083010, toyocamycin and a series of MKC compounds, whilst kinase pharmacological inhibitors that in turn inhibit the RNase include compound 3 and, although unclear as to its effect on IRE1 activity, sunitinib [10]. The description of an allosteric IRE1 RNase inhibitory mechanism by ATP competitive ligands was provided through the discovery of kinase-inhibiting RNase attenuators (KIRAs) showing that the inhibition of the kinase site may have an inhibitory effect on the RNase activity [11,12]. In addition to those pharmacological inhibitors, we discovered that peptide fragments derived from the IRE1 cytosolic domain itself affected its oligomerisation and subsequent RNase activity [13,14]. Consequently, we postulated that these fragments could pose as attractive 'blueprints' for the discovery of IRE1 modulators since structurally homologous, and hence complementary, to regions of IRE1 itself, they would confer higher selectivity for IRE1 binding and reduced off-target effects. Here, using a structural homology approach comprising molecular docking and pharmacophore analysis, we identify peptides and FDA-approved compounds based on IRE1 peptide fragment interactions. We demonstrate that they have an impact on IRE1 activity *in vitro* and in human cell models of glioblastoma multiforme (GBM) whilst at the same time addressing the clinical relevance of IRE1 inhibition in oncology by demonstrating that the administration of these compounds sensitises human cancer cells to chemotherapy. Furthermore, since the FDA-approved compounds that we identified are in widely available clinical use, this also sheds light onto reported side effects that hence could potentially be attributed to IRE1 inhibition.

Results

Our previous studies indicated that large (18–50 amino acid long) peptides derived from the cytosolic domain of IRE1 could affect its oligomerisation and subsequent RNase activity [13]. Developing these structures further was an attractive notion due to the sequence homology to IRE1 and hence their projected affinity and specificity of binding on it. However, such peptides (termed F6, covering residues 690–744 of the IRE1 cytosolic domain; Scheme 1), even in their reduced 18 amino acid form (termed P4, structure seen in Fig. 1A and [13]), presented a plethora of issues such as bioavailability, proteasomal degradation, sheer size, crossing the blood–brain barrier and stability when considering use in *in vivo* settings. As such, it was pertinent to reduce the size of these fragments and also identify nonpeptide candidates that could substitute the peptide structures and thus overcome peptide-related issues (Scheme 1).

Small IRE1-derived peptides dock onto the ATP-binding pocket of IRE1 with high affinity *in silico*

To address this, a library of overlapping tetra- and pentapeptides derived from the IRE1 amino acid sequences previously identified to be biologically active [13] was generated *in silico*. This peptide library was then docked onto the kinase domain of IRE1 using the Glide docking tool in Schrödinger [15] (Fig. 1A). To avoid docking bias, the grid generated for docking this library of peptides had its centroid in the middle of the kinase domain rather than at the ATP-binding pocket. However, the peptides preferentially occupied this active site. At this point, having explored potential docking of the peptide library on the entire kinase domain it was evident that small peptides derived from the IRE1 kinase structure would preferentially dock onto the ATP-binding pocket. Upon exploration of the binding pocket and docking of the peptide library,

17424658, 2021, 3, Downloaded from https://febs.onlinelibrary.wiley.com/doi/10.1111/febs.15372 by Universite de Rennes, Wiley Online Library on [23/01/2023]. See the Terms and Conditions (https://onlinelibrary.wiley.com/terms-and-conditions) on Wiley Online Library for rules of use; OA articles are governed by the applicable Creative Commons License

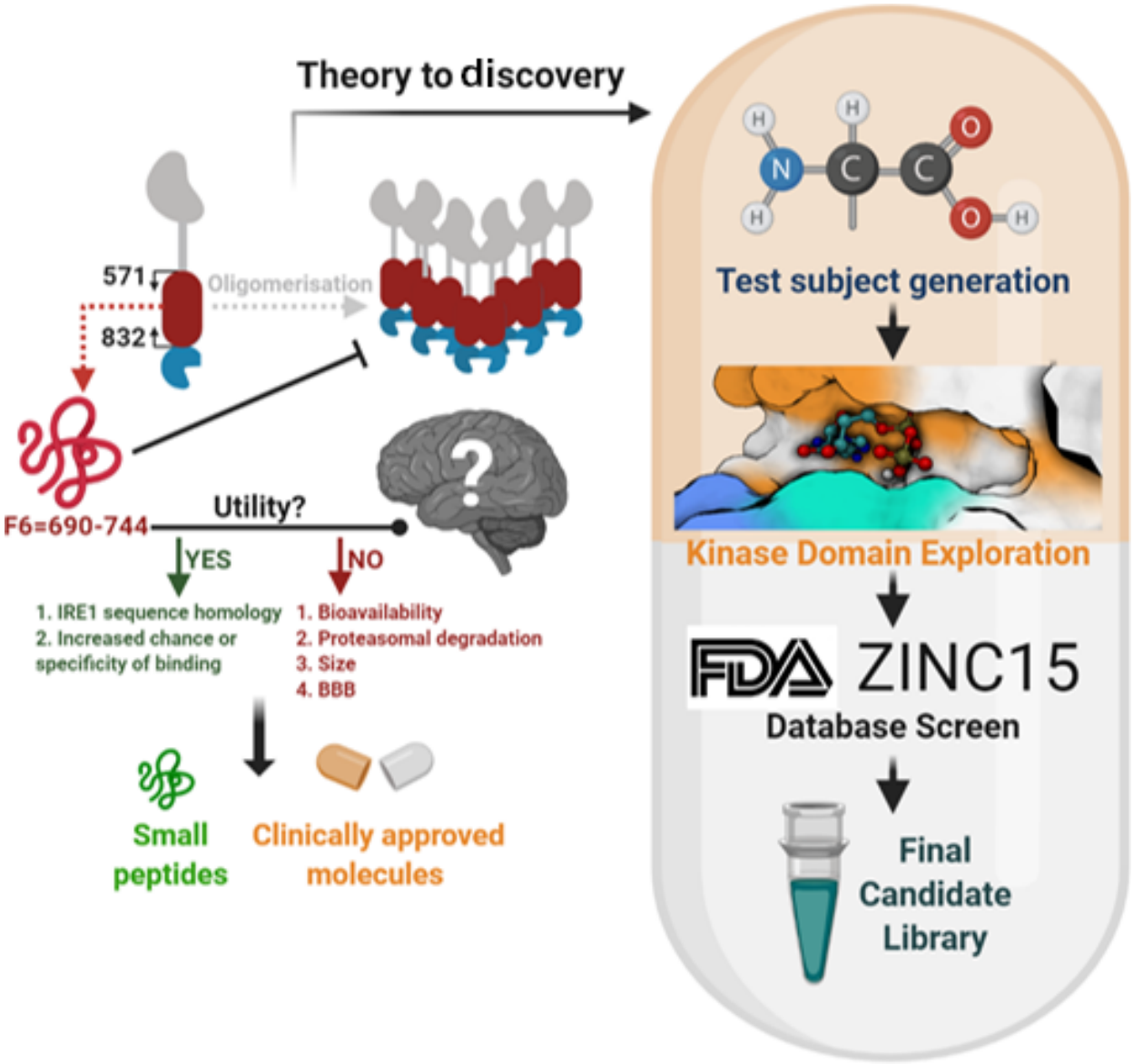

Scheme 1. IRE1 modulators: From theory to discovery. Schematic explaining the rationale of the current investigation and computational workflow from assessing known information (left side) to the work carried out (right side). IRE1 is a transmembrane dual enzyme with its cytosolic part comprising of a kinase (red) and a ribonuclease (blue) domain [1]. The kinase domain is encompassed within residues 571 and 832. IRE1 is in monomeric form when inactive but when activated it trans-autophosphorylates and oligomerises to splice XBP1 mRNA or cleave miRNAs and mRNAs through RIDD [2]. It was shown that a fragment of the kinase domain encompassed between residues 690 and 744, named F6, inhibited IRE1 oligomerisation [13] with functional consequences leading to the question: Could this be used in a higher-order brain cancer model? To overcome issues such as bioavailability and proteasomal degradation and enable passage across the blood–brain barrier, one would need either smaller peptidic (green) or clinically approved (orange) molecules. This led to the current investigation (pill box; top to bottom) where small peptides derived from F6 were generated as test subjects, the kinase domain was explored for docking opportunities, and the best docking test subjects were optimised and used to filter through a database of FDA-approved molecules. The final library of small peptides and clinically approved molecules optimally binding onto IRE1 was subsequently used for further investigation.

peptides exhibiting superior docking scores were chosen for further modification. These modifications included single amino acid substitutions upon alanine scanning, chirality orientation changes and cyclisation attempts. The modified peptides and the original library were redocked to obtain small peptides with

17424658, 2021, 3, Downloaded from https://febs.onlinelibrary.wiley.com/doi/10.1111/febs.15372 by Universite de Rennes, Wiley Online Library on [23/01/2023]. See the Terms and Conditions (https://onlinelibrary.wiley.com/terms-and-conditions) on Wiley Online Library for rules of use; OA articles are governed by the applicable Creative Commons License

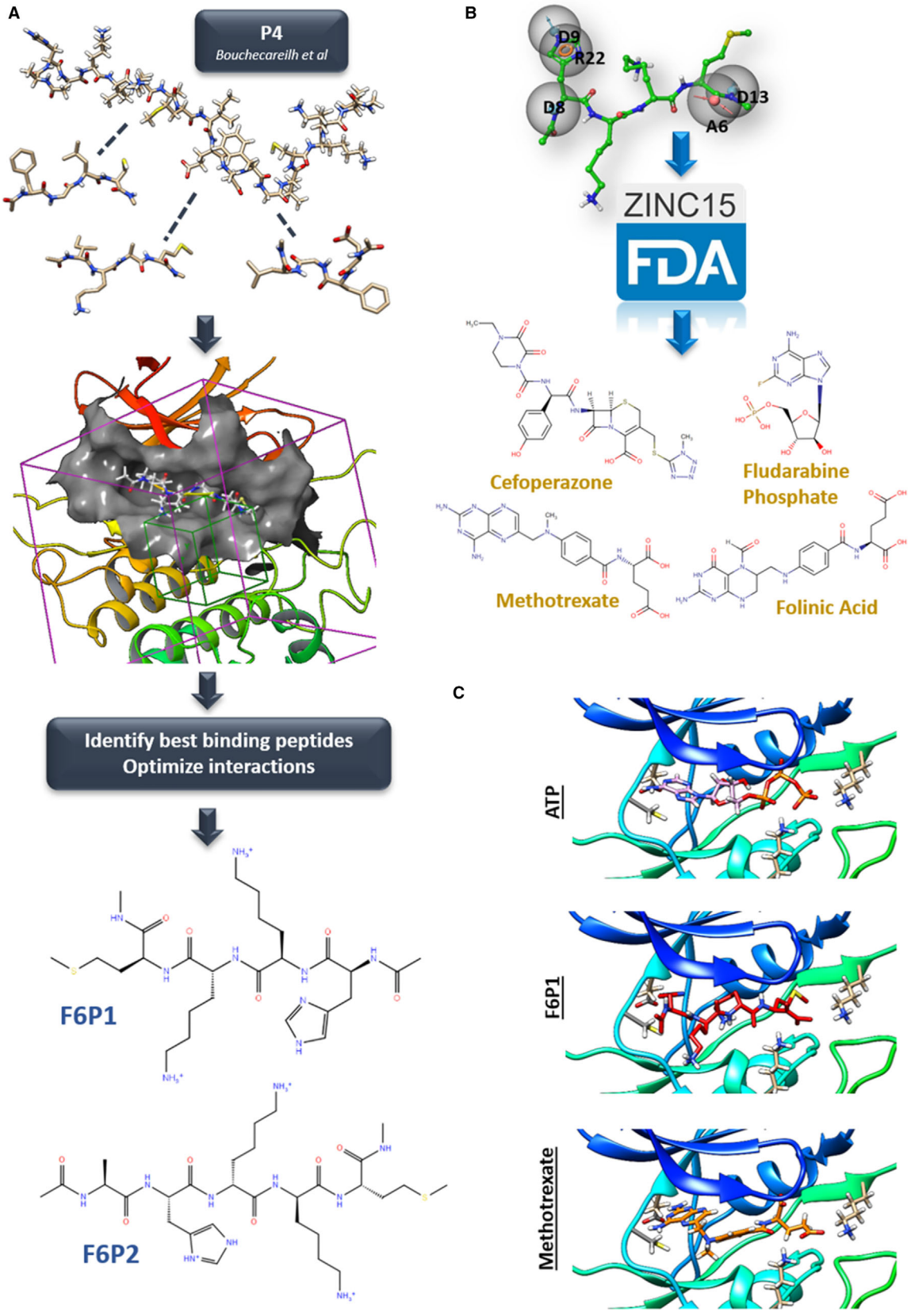

17424658, 2021, 3, Downloaded from https://febs.onlinelibrary.wiley.com/doi/10.1111/febs.15372 by Universite de Rennes, Wiley Online Library on [23/01/2023]. See the Terms and Conditions (https://onlinelibrary.wiley.com/terms-and-conditions) on Wiley Online Library for rules of use; OA articles are governed by the applicable Creative Commons License

Fig. 1. Small IRE1-derived peptides dock onto the ATP-binding pocket of IRE1 with high affinity *in silico* and are used to identify FDA-approved compounds as IRE1 inhibitors. (A) Structure of large IRE1 fragment P4 that was determined to affect IRE1 oligomerisation as described in ref. [13] as well as three example small peptides derived from its sequence and the grid constructed to guide docking of these molecules on the IRE1 F6 region (part of the kinase domain; PDB ID 3P23). Peptide optimisation and redocking led to the identification of the two F6-derived small peptides with better docking scores than ATP named F6P1 and F6P2 (Table 1) that were chosen for further investigation. (B) Generation of a pharmacophore-binding hypothesis utilising F6P1 and F6P2 (F6P1 used as example here) screened against the ZINC15 FDA-approved database followed by docking onto the IRE1 structure using the grid described in (A). Comparing docking scores to ATP and F6P1/2, four FDA-approved molecules were selected for further investigation. (C) Examples of docking of candidates in the ATP-binding pocket of IRE1 (PDB ID 3P23) showing ATP the control, F6P1 as a peptide example and methotrexate as an FDA-approved therapeutic. Structures in figure were generated using Maestro Suites 2015-2018 (Schrödinger Release 2018-4: Schrödinger, LLC, 2018).

maximal docking scores compared with ATP (PDB structure 3P23) or sulfonamide (PDB structure 4U6R). Out of this process, the two candidates with the best docking scores (one tetrapeptide F6P1 and one pentapeptide F6P2) were chosen to be further investigated (Fig. 1A, Table 1).

Identification of FDA-approved drugs binding to the ATP-binding pocket of IRE1 with high affinity *in silico*

Binding hypotheses based on pharmacophore modelling between the kinase domain and these strongly binding modified peptides were computationally generated (Fig. 1B). We used the obtained pharmacophore hypotheses to screen a database of FDA-approved molecules (ca. 1400 compounds) to yield structures with theoretically similar binding capabilities as the small peptides [18] (Fig. 1B). The screen outcomes were then docked onto the ATP-binding pocket, and the candidates with the best docking scores along with the best scoring peptides described in Fig. 1A formed a final list of candidates to be further tested *in vitro* for their capacity to alter IRE1 RNase activity. The organic molecules thus identified included the FDA-approved compounds methotrexate, folinic acid, cefoperazone and fludarabine phosphate (Fig. 1B and Table 1). All docking was performed using standard precision (SP) and extra precision (XP) [19] and the OPLS-2005 force field [20].

Table 1. *In silico* and *in vitro* data for small peptides and clinically approved organic molecules derived from the IRE1 structure. Data are presented for compounds used as controls for the *in silico* docking such as ATP for IRE1 crystal PDB structure 3P23 [16] and sulfonamide for PDB structure 4U6R [17]. All compounds obtained from the *in silico* small peptide design or FDA-approved compound database screen were docked onto both receptors, and the scores are presented here (scores in kcal·mol^{-1} are the result of SP (standard precision) docking with Maestro version 2015). The calculated *in vitro* IC50s are extrapolated from percentage inhibition of IRE1 activity curves as shown in Figs 3 and 4. The final four columns are dedicated to toxicity IC50s for U87 and RADH87 GBM cell lines as shown in Figs 5A and 6A, and U87 and RADH87 sensitisation to TMZ in the presence of nontoxic doses of each compound (Figs 5F and 6F).

Compound	Compound type	Clinical use	IRE1 target	Kinase receptor (PDB)	Docking score (kcal·mol^{-1})	*In vitro* IC50 (μM)	Toxicity (μM)		TMZ IC50 (μM)	
							U87	RADH87	U87	RADH87
ATP	Control	N/A		3P23	−8.044	N/A	N/A	N/A	N/A	N/A
Sulfonamide				4U6R	−7.815					
MKC8866		N/A		N/A	N/A	0.409	N/A	N/A	N/A	N/A
Temozolomide		Chemotherapy		N/A	N/A	N/A	N/A	N/A	> 2500	> 2500
F6P1	Peptide	N/A	Kinase	3P23	−9.442	3.837	N/A	N/A	N/A	N/A
				4U6R	−7.783					
F6P2	Peptide	N/A	Kinase	3P23	−9.260	28.621	N/A	N/A	N/A	N/A
				4U6R	−9.125					
Cefoperazone	Cephalosporin	Bacterial infection	Kinase	3P23	−5.211	0.421	> 1000	996.0	1786	1225
				4U6R	−8.090					
Methotrexate	Antifolate	Chemotherapy	Kinase	3P23	−9.478	1.647	> 1000	132.4	1957	2309
				4U6R	−4.323					
Folinic acid	Folic acid derivative	Chemotherapy	Kinase	3P23	−8.838	0.552	> 1000	> 1000	2124	2824
				4U6R	−5.546					
Fludarabine phosphate	Purine analogue	Chemotherapy	Kinase	3P23	−8.188	0.245	27.03	66.59	2434	1850
				4U6R	−6.865					

17424658, 2021, 3, Downloaded from https://febs.onlinelibrary.wiley.com/doi/10.1111/febs.15372 by Universite de Rennes, Wiley Online Library on [23/01/2023]. See the Terms and Conditions (https://onlinelibrary.wiley.com/terms-and-conditions) on Wiley Online Library for rules of use; OA articles are governed by the applicable Creative Commons License

Methotrexate is used in chemotherapy against a variety of cancers and disease-modifying treatment in a plethora of autoimmune disorders through two separate mechanisms. In cancer, it serves as a folic acid antagonist [21], whilst in disorders such as rheumatoid arthritis it interferes with purine and pyrimidine precursors needed for cell proliferation [22]. Folinic acid (or leucovorin) is coprescribed with methotrexate to reduce methotrexate side effects [23]. Cefoperazone is a third-generation antibiotic from the cephalosporin family causing bacterial cell wall lysis [24], whilst fludarabine phosphate is a chemotherapeutic used in haematological malignancies by disrupting DNA synthesis [25]. As exemplified by methotrexate in Fig. 1C, the FDA-approved compounds align well in the IRE1 ATP-binding pocket with the 2,4-diaminopteridine unit attaining the position of the adenine in ATP, and the oxygen-rich pentanedioic 'tail' aligning along the phosphate-binding region of the pocket. The similarity in interactions is also seen from the 2D interaction plots (Fig. 2). Interestingly, of the different compounds obtained, it is only cefoperazone that was identified as a key binder from the sulfonamide-bound crystal structure 4U6R, which is slightly distorted relative to the ATP-bound form, a distortion that has been claimed to be the key factor of the KIRA-like compound ability to attenuate RNase activity. The remaining compounds were obtained as top hits upon binding to the ATP-binding form of IRE1 (PDB ID 3P23), yet, as seen below (Section FDA-approved drugs predicted to bind the IRE1 kinase domain from in silico analysis, affect IRE1 activity in vitro and sensitise GBM cellular models to TMZ), are nonetheless highly efficient in blocking RNase activity. This indicates that the mechanism of action of the KIRA compounds is slightly more complex than only dependent on that the induced distortions affect oligomerisation [26].

Small IRE1-derived peptides modulate IRE1 activity *in vitro* and in cultured cells

The ability of F6P1 and F6P2 to bind IRE1 *in vitro* was tested using microscale thermophoresis (MST) assays. Indeed, the MST investigation showed dose–response binding of these molecules to recombinant IRE1 with K_d values in the 10–30 μM range. Specifically, F6P1 showed a higher binding affinity for IRE1 compared with F6P2 (Fig. 3A,B). Subsequently, F6P1 and F6P2 were tested in an *in vitro* cleavage assay as previously described [27] using MKC8866 as a positive control (IC50 0.41 μM) and reaction buffer as a negative control in the presence of recombinant IRE1, ATP, DTT and a fluorescent Cy5-BHQ3 probe (Fig. 3C,D and Table 1). Both F6P1 and F6P2 show some degree of IRE1 RNase inhibition with IC50s calculated in the 3-30 μM range, F6P1 showing more potent inhibition than F6P2 (Fig. 3C,D and Table 1) recapitulating the relationship seen between the MST K_d values for the two peptides. We then investigated the potential of these peptides to affect IRE1 function in a cell model. Increasing concentrations of each peptide were transfected in HEK293T cells over 4 h, and subsequently, the cells were treated with 1 $\mu g \cdot mL^{-1}$ tunicamycin for a further 4 h. XBP1 mRNA splicing was then tested as a marker of IRE1 RNase activity. As observed *in vitro*, both peptides attenuated tunicamycin-induced IRE1-dependent XBP1 mRNA non-conventional splicing in HEK293T cells in a dose-dependent manner (Fig. 3E).

FDA-approved drugs predicted to bind the IRE1 kinase domain from *in silico* analysis, affect IRE1 activity *in vitro* and sensitise GBM cellular models to TMZ

Having shown that small peptides derived from the kinase domain sequence of IRE1 are capable to bind onto and inhibit IRE1 activity *in vitro* and in a cell model, we next tested the hits from the screened FDA-approved drugs as above, this time including both primary (RADH87 [28]) and common (U87) human GBM lines. Once again, we monitored IRE1 activity in the presence of increasing concentrations of inhibitors in our *in vitro* cleavage assay. Interestingly, all compounds showed a varying degree of inhibition (Fig. 4B–E) confirming the hypothesis that the structure and binding based *in silico* screening yielded candidates with similar properties to the peptides when considering properties of IRE1 inhibition. IC50 values for IRE1 inhibition were determined and found to be in the 0.2–2 μM range (Fig. 4 and Table 1), that is much more potent than the peptides, and of similar order of magnitude as MKC8866 (IC50 0.41 μM) although with different inhibition profiles.

Since the majority of the compounds are therapeutics with known side effects, a toxicity screen was carried out in U87 and RADH87 GBM cells with increasing concentrations of each compound utilising a cell viability assay (WST1). A toxicity IC50 value was calculated for each compound, and thus, subtoxic doses were determined for any and all subsequent assays for each cell line used (Figs 5A and 6A; Tables 1 and 2). It was noted that fludarabine phosphate exhibited high toxicity already at low doses. To verify the ability of the compounds to act as IRE1

17424658, 2021, 3, Downloaded from https://febs.onlinelibrary.wiley.com/doi/10.1111/febs.15372 by Universite de Rennes, Wiley Online Library on [23/01/2023]. See the Terms and Conditions (https://onlinelibrary.wiley.com/terms-and-conditions) on Wiley Online Library for rules of use; OA articles are governed by the applicable Creative Commons License

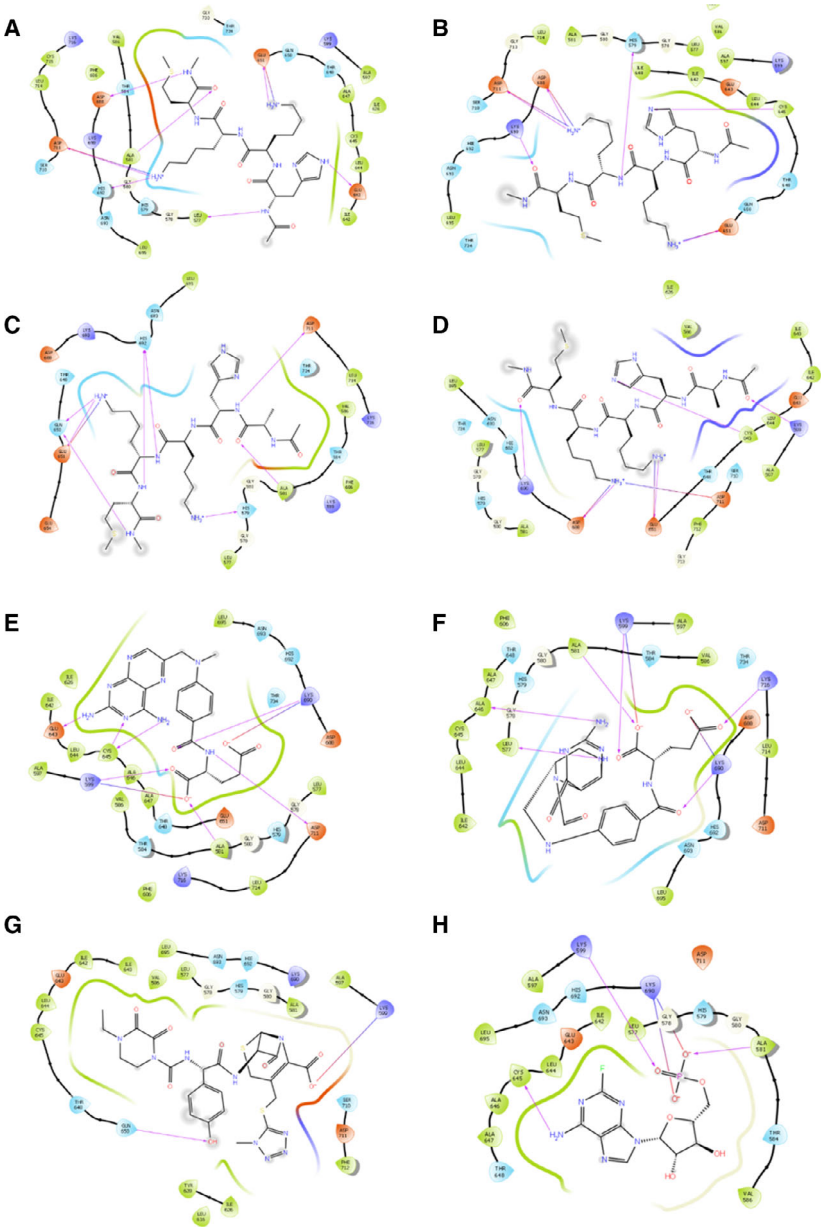

Fig. 2. 2D Ligand interaction maps for peptides F6P1 and F6P2, and the identified FDA-approved compounds, docked to the IRE1 ATP kinase-binding sites. F6P1 in the ATP kinase-binding pocket of (A) PDB ID 3P23 and (B) PDB ID 4U6R. F6P2 in the ATP kinase-binding pocket of (C) PDB ID 3P23 and (D) PDB ID 4U6R. (E) Methotrexate in the 3P23 ATP kinase-binding pocket. (F) Folinic acid in the 3P23 ATP kinase-binding pocket. (G) Cefoperazone in the 4U6R ATP kinase-binding pocket. (H) Fludarabine phosphate in the 3P23 ATP kinase-binding pocket. Structures in Figure were generated using Maestro Suites 2015-2018 (Schrödinger Release 2018-4: Schrödinger, LLC, 2018).

inhibitors by impacting on IRE1 kinase activity, we next treated U87 and RADH87 cells with subtoxic doses of each compound for 24 h and measured the ratio of phospho-IRE1 (anti-P-S724) over total IRE1 compared with the untreated samples. The majority of our compounds significantly reduced IRE1 autophosphorylation and hence potentially its activity at the protein level, with some intercell line variability (Figs 5B,C and 6B,C).

To test the ability of the identified compounds to inhibit IRE1 activity in human GBM cell models as well as determine the effect they may have upon induction of ER stress with different stressors, we treated U87 and RADH87 cells with subtoxic doses of the FDA-approved compounds in the presence of 1 $\mu g \cdot mL^{-1}$ tunicamycin or 0.5 $\mu g \cdot mL^{-1}$ SubAB toxin [29] for 24 and 1.5 h, respectively (Figs 5D,E and 6D, E). Tunicamycin is an antibiotic that causes ER stress via blocking N-linked protein glycosylation, whilst SubAB acts as a serine protease cleaving BiP/GRP78 [30], a chaperone essential for the recognition of unfolded protein load increase in the ER [31]. All compounds tested in the presence of tunicamycin in U87 or RADH87 cells decreased XBP1 mRNA splicing over time. The induction profiles of both common (U87) and primary (RADH87 [3]) GBM lines in the

17424658, 2021, 3, Downloaded from https://febs.onlinelibrary.wiley.com/doi/10.1111/febs.15372 by Universite de Rennes, Wiley Online Library on [23/01/2023]. See the Terms and Conditions (https://onlinelibrary.wiley.com/terms-and-conditions) on Wiley Online Library for rules of use; OA articles are governed by the applicable Creative Commons License

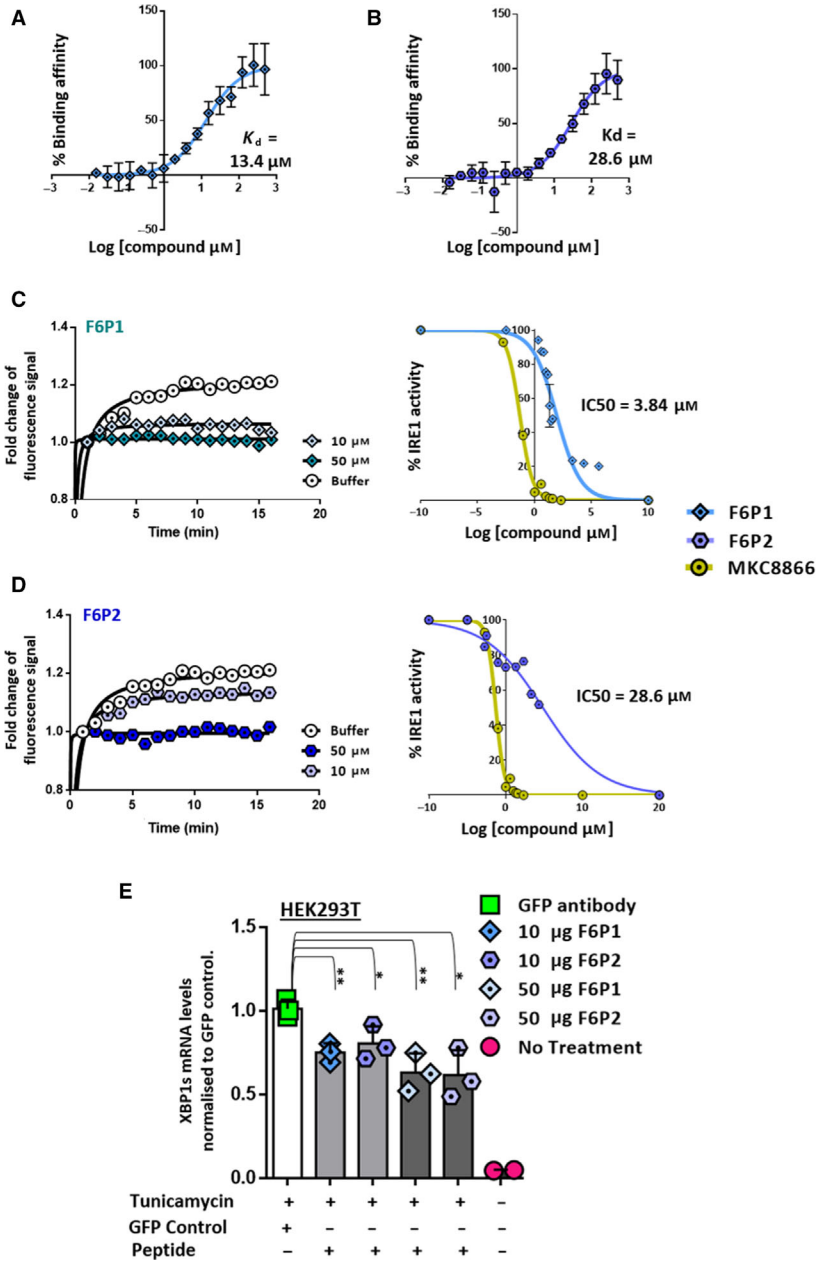

Fig. 3. Small IRE1-derived peptides modulate IRE1 activity *in vitro* and in cultured cells. (A, B) Dose-dependent binding affinity of F6P1 (A) and F6P2 (B) based on MST signal measurements. Results are shown as mean ± SD (n = 4). (C, D) Activity of IRE1 in the presence of F6P1 (C) and F6P2 (D) compared with MKC8866 stemming from FRET signal upon fluorescent probe cleavage over 25-min incubation. Representative curves of peptides and control. MKC8866 was used as a comparator for efficacy of RNase activity blocking. (E) HEK293T cells were transfected with increasing concentrations of F6P1 or F6P2 and treated with tunicamycin. XBP1s mRNA levels were measured after a 4-h treatment as a measure of IRE1 RNase activity. An ordinary one-way ANOVA was performed to check for statistical significance with the addition of Dunnett's multiple comparison test comparing all individual clusters to GFP. Significance summary based on 95% CL of diff.: ** = 0.02809 to 0.4950; * = 0.1477 to 0.6146; ** = −0.02516 to 0.4418; * = 0.1633 to 0.6302. Results are shown as mean ± SD (n = 3).

presence of tunicamycin were similar with the starkest differences seen at 16 and 24 h of treatment (Figs 5D and 6D). ER stress induction with the SubAB toxin was much faster with maximal XBP1s expression observed at 1.5 h after treatment. No change in XBP1 splicing was observed in the primary human line (RADH87), but this could be attributed to the fact that human cells are deficient for Neu5Gc, a sialic acid displayed on cell surface glycoconjugates that is recognised by the toxin B subunit with high specificity [32] triggering internalisation of the holotoxin. As such, an effect of this toxin on primary human cells is far less likely than one on commonly available lines such as U87 (Figs 5E and 6E). Such conserved effect of the molecules across different types of stress and cell lines solidifies the notion that compounds identified in our study are true inhibitors of IRE1 activity.

IRE1 has been shown to play a major role in GBM pathogenesis and pathophysiology both in animal models and in human tumours [3]. It thus stands to reason that blocking IRE1 activity would be an attractive target in GBM treatment. However, when considering the clinical state of GBM or in fact any tumour in a systemic setting it is evident that sustained

17424658, 2021, 3, Downloaded from https://febs.onlinelibrary.wiley.com/doi/10.1111/febs.15372 by Universite de Rennes, Wiley Online Library on [23/01/2023]. See the Terms and Conditions (https://onlinelibrary.wiley.com/terms-and-conditions) on Wiley Online Library for rules of use; OA articles are governed by the applicable Creative Commons License

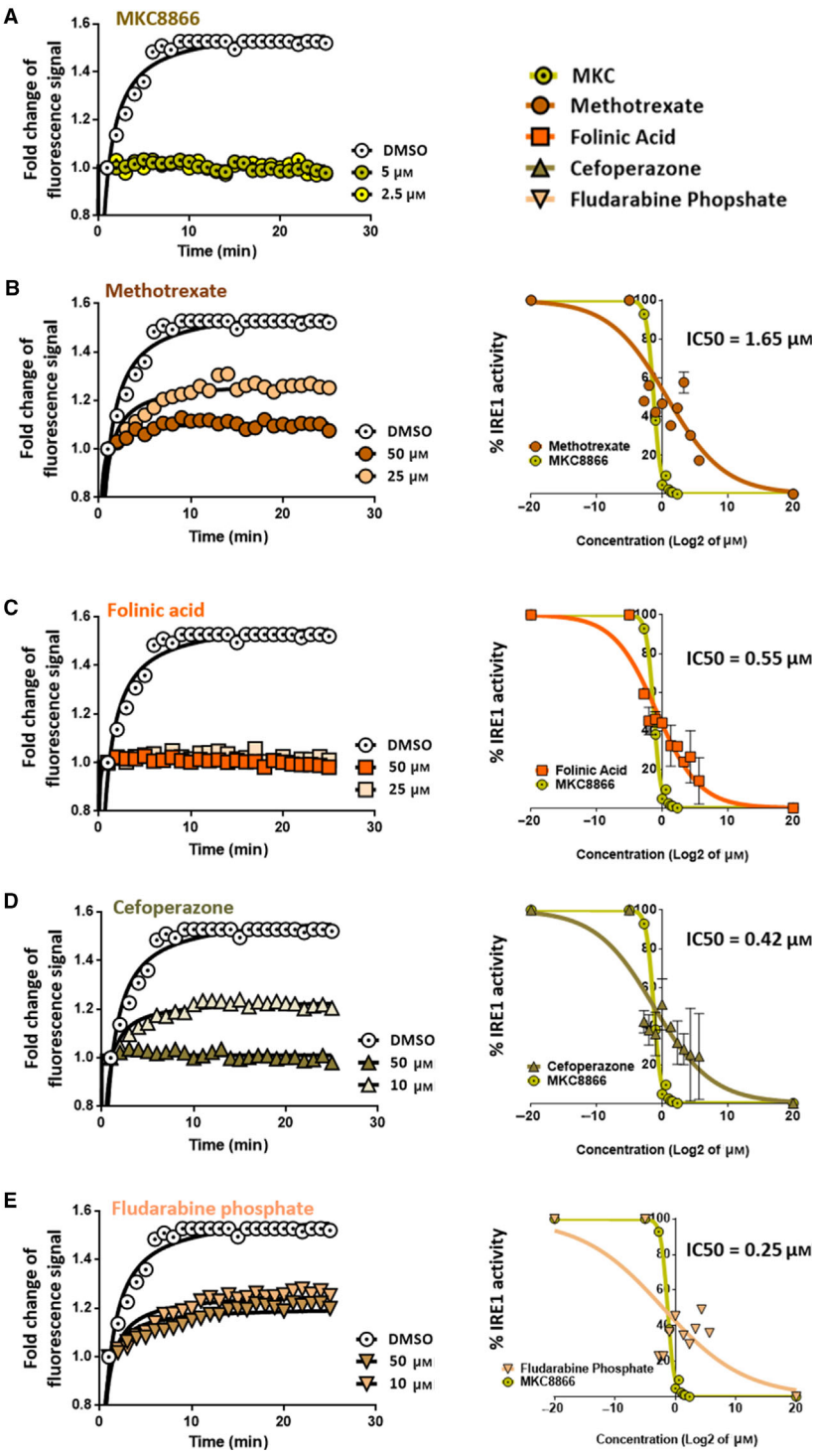

Fig. 4. *In vitro* fluorescence cleavage assay design and validation, and cleavage assay fluorescence curves. RNA probe including a 3′ Cy5 fluorescent dye and a 5′ BHQ3 quencher was incubated with recombinant IRE1. Probe cleavage leads to an increase in fluorescence. (A) MKC8866 was used as a comparator for efficacy of RNase activity blocking. (B–E) Representative curves of varying concentrations of molecules and control (DMSO for FDA-approved molecules). Activity of IRE1 in the presence of methotrexate, folinic acid, cefoperazone and fludarabine phosphate compared with MKC8866 stemming from FRET signal upon fluorescent probe cleavage over 25-minute incubation. Each compound is listed at the top of the respective curve. Results are shown as mean ± SD (n = 4) for all activity curves bar fludarabine phosphate which represents n = 2.

inhibition of IRE1 may have adverse rather than beneficial effects. Consequently, a far more attractive hypothesis would be to sensitise tumours to the standard of care, the combination of chemotherapy and radiotherapy. In such a scenario, tumour cells would be swiftly removed without the need for a prolonged exposure to IRE1 inhibition and potentially without prolonged exposure to highly toxic-alkylating agents such as TMZ. To this end, we tested the effect of the IRE1-inhibiting compounds identified herein in our

17424658, 2021, 3, Downloaded from https://febs.onlinelibrary.wiley.com/doi/10.1111/febs.15372 by Universite de Rennes, Wiley Online Library on [23/01/2023]. See the Terms and Conditions (https://onlinelibrary.wiley.com/terms-and-conditions) on Wiley Online Library for rules of use; OA articles are governed by the applicable Creative Commons License

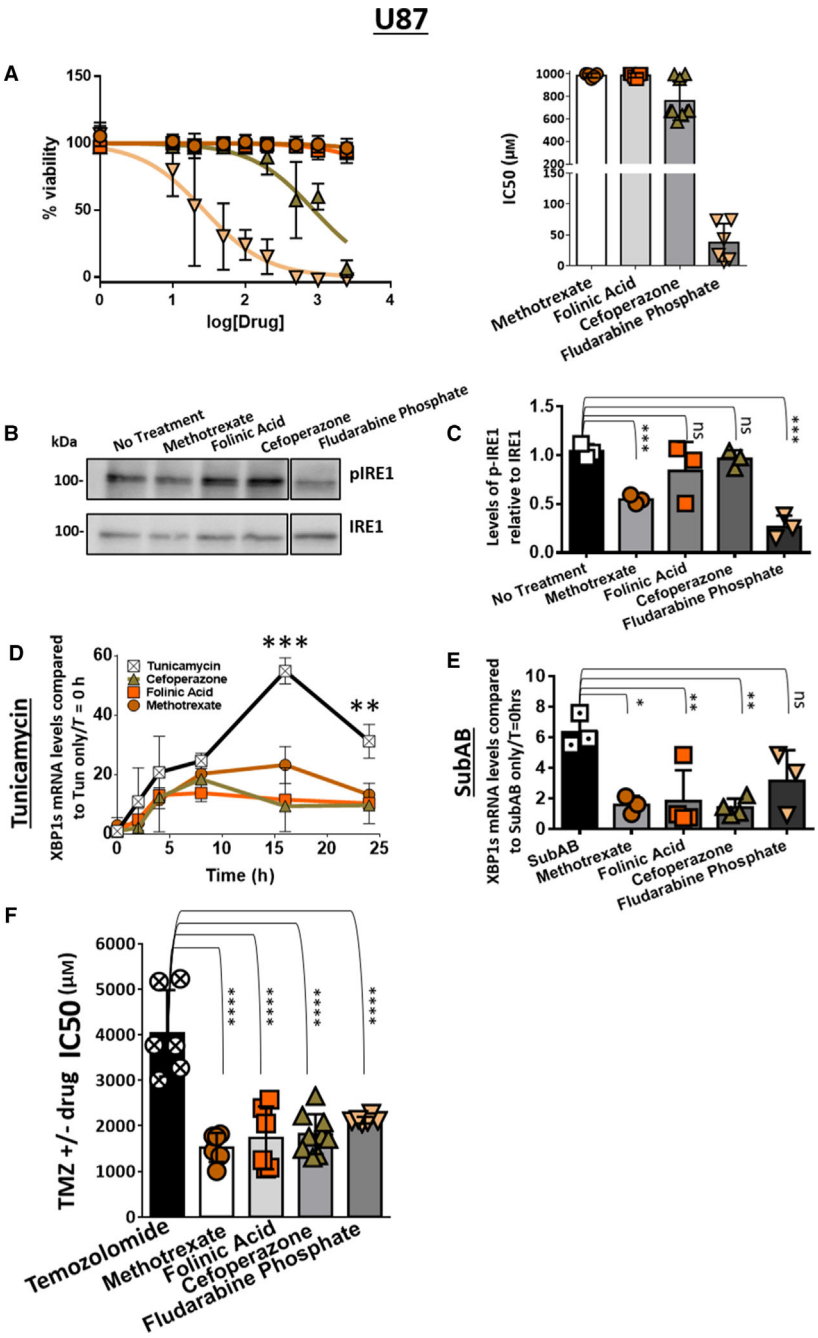

cellular GBM models when treated with TMZ. Guided by the above toxicity assays (Figs 5A and 6A), cells were treated with subtoxic doses of methotrexate, folinic acid, cefoperazone or fludarabine phosphate (Table 2) and then subjected to increasing concentrations of TMZ (0–2500 μM) in the same temporal manner as with the toxicity investigation above. Kill curves were once again calculated and the IC50 of TMZ for U87 and RADH87 cells in the presence of each compound inferred (Table 1). All of the tested compounds significantly sensitised both commonly available and primary GBM cells to TMZ (Figs 5F and 6F).

Discussion

Herein, we have uncovered a group of molecules that inhibit IRE1 activity and sensitise GBM cells (both

17424658, 2021, 3, Downloaded from https://febs.onlinelibrary.wiley.com/doi/10.1111/febs.15372 by Universite de Rennes, Wiley Online Library on [23/01/2023]. See the Terms and Conditions (https://onlinelibrary.wiley.com/terms-and-conditions) on Wiley Online Library for rules of use; OA articles are governed by the applicable Creative Commons License

Fig. 5. FDA-approved drugs predicted to bind the IRE1 kinase domain *in silico*, affect IRE1 activity *in vitro* and sensitise commonly available GBM cellular models to TMZ. (A) Toxicity IC50s for each of the four inhibitors in U87 cells. Results are shown as mean ± SD ($n = 3$). Compounds not showing toxicity (flat curves) are capped to IC50s of 1000 μM. (B) Representative blot of U87 cell treatment, blotted for IRE1 and phospo-IRE1. $N = 3$ separate biological repeats were carried out, quantification of which can be seen in C. (C) Protein levels of IRE1 and phospho-IRE1 in U87 cells treated with methotrexate, folinic acid, cefoperazone and fludarabine phosphate over 24 h. Fold change in protein expression between IRE1 and phospho-IRE1 is represented in bar chart form normalised to the corresponding untreated cells. Results are shown as mean ± SD ($n = 3$). Unpaired t-tests were performed to test for statistical significance between each condition and untreated. ***$P = 0.0006$ for both methotrexate and fludarabine phosphate. (D) XBP1s mRNA levels upon treatment with 1 $\mu g \cdot mL^{-1}$ tunicamycin over 24 h normalised to untreated U87 cells. Results are shown as mean ± SD ($n = 3$). Multiple t-tests were performed to test for statistical significance between each condition and control. ***$P = 0.00196$ 16 h, **$P = 0.00562$ 24 h. (E) XBP1s mRNA levels upon treatment with 0.5 $\mu g \cdot mL^{-1}$ SubAB toxin after 1.5 h normalised to untreated U87 cells. Results are shown as mean ± SD methotrexate, fludarabine phosphate ($n = 3$), folinic acid and cefoperazone ($n = 4$). An ordinary one-way ANOVA was performed to check for statistical significance with the addition of Dunnett's multiple comparison test comparing all individual clusters to control. Significance summary based on 95% CL of diff.: * = 1.019–8.500 methotrexate; ** = 1.013–8.011 folinic acid; ** = 1.430–8.427 cefoperazone. (F) TMZ IC50s in the presence of nontoxic doses of IRE1 inhibitors in U87 cells. Results are shown as mean ± SD ($n = 6$). An ordinary one-way ANOVA was performed to check for statistical significance with the addition of Dunnett's multiple comparison test comparing all individual clusters to control. Significance summary based on 95% CL of diff.: **** = 1705–3316 methotrexate; **** = 1494–3105 folinic acid; **** = 1482–2953 cefoperazone; **** = 1106–2717 fludarabine phosphate.

established and primary lines) to TMZ chemotherapy when used at subtoxic doses. Our investigation offers major advantages to the pursuit of a solution to the temporally rapid progression and dismal end of many cancers such as GBM, pancreatic cancer and TNBC, as well as the accumulation of information with respect to off-target actions of many compounds in clinical use.

We designed a drug discovery process by which, using datasets of already existing molecules, compounds that can inhibit IRE1 activity *in silico*, *in vitro* and in cell-based models could be identified. In an ever-increasingly financially competitive environment of novel compound recognition, such approaches could prove an indispensable tool to bypass the need for new synthesis and thus fast-track drug repurposing and clinical benefit (Scheme 1). Secondly, we identify novel modes of action for molecules already in abundant clinical use. Methotrexate, for example, is on the List of Essential Medicines [33] with dual mechanisms of action in various malignancies and autoimmune disorders. Its interference with IRE1 activity could severely impact its efficacy as a therapeutic as well as potentially open avenues of research into mechanisms of alleviating its side effects [34] that, based on the current findings, may be the result of its potential as a UPR disruptor.

We have furthermore identified already clinically approved therapeutics that could potentially have a beneficial effect on GBM, a disease in dire need for improved clinical options. Such discoveries are of great benefit to clinical trial design as they can be put straight into the clinic with much reduced temporal and financial burden onto the design of the trial itself. This means that patients could benefit from such insights into an expedient manner. Alternative biophysical approaches such as mass spectrometry [35] or NMR could provide crucial pieces of information to corroborate the information received from the current study and validate these new series of ligands as novel class of IRE1 endoribonuclease inhibitors, to be complemented with the already available hydroxy–aryl–aldehyde and KIRA classes of compounds [12,36].

In conclusion, through the structural interrogation of the IRE1 kinase catalytic domain and subsequent *in silico* screen, we have identified four clinically approved molecules that inhibit IRE1 RNase activity *in vitro* and in human GBM cell models, and sensitise them to the established GBM chemotherapy treatment, temozolomide. As such, we further annotate the mode of action of widely used therapeutics and map their potential use in drug-repurposing scenarios as IRE1 modulators.

Materials and methods

Materials

Recombinant human IRE1 cytosolic domain (11905-HNCB) was from Sino Biological Europe GmbH (Eschborn, Germany). The fluorescent probe (Cy3-CAUGUCCGCAGCGCAUG-BHQ3) used for the *in vitro* IRE1 RNase assay was purchased from Eurogentec (Liège, Belgium). Tunicamycin was purchased from Calbiochem (Merck KGaA, Darmstadt, Germany). SubAB toxin was purified from recombinant *E. coli* as previously described [37]. All the other inhibitors were synthesised by and purchased from companies outlined as follows. Peptides, F6P1

17424658, 2021, 3, Downloaded from https://febs.onlinelibrary.wiley.com/doi/10.1111/febs.15372 by Universite de Rennes, Wiley Online Library on [23/01/2023]. See the Terms and Conditions (https://onlinelibrary.wiley.com/terms-and-conditions) on Wiley Online Library for rules of use; OA articles are governed by the applicable Creative Commons License

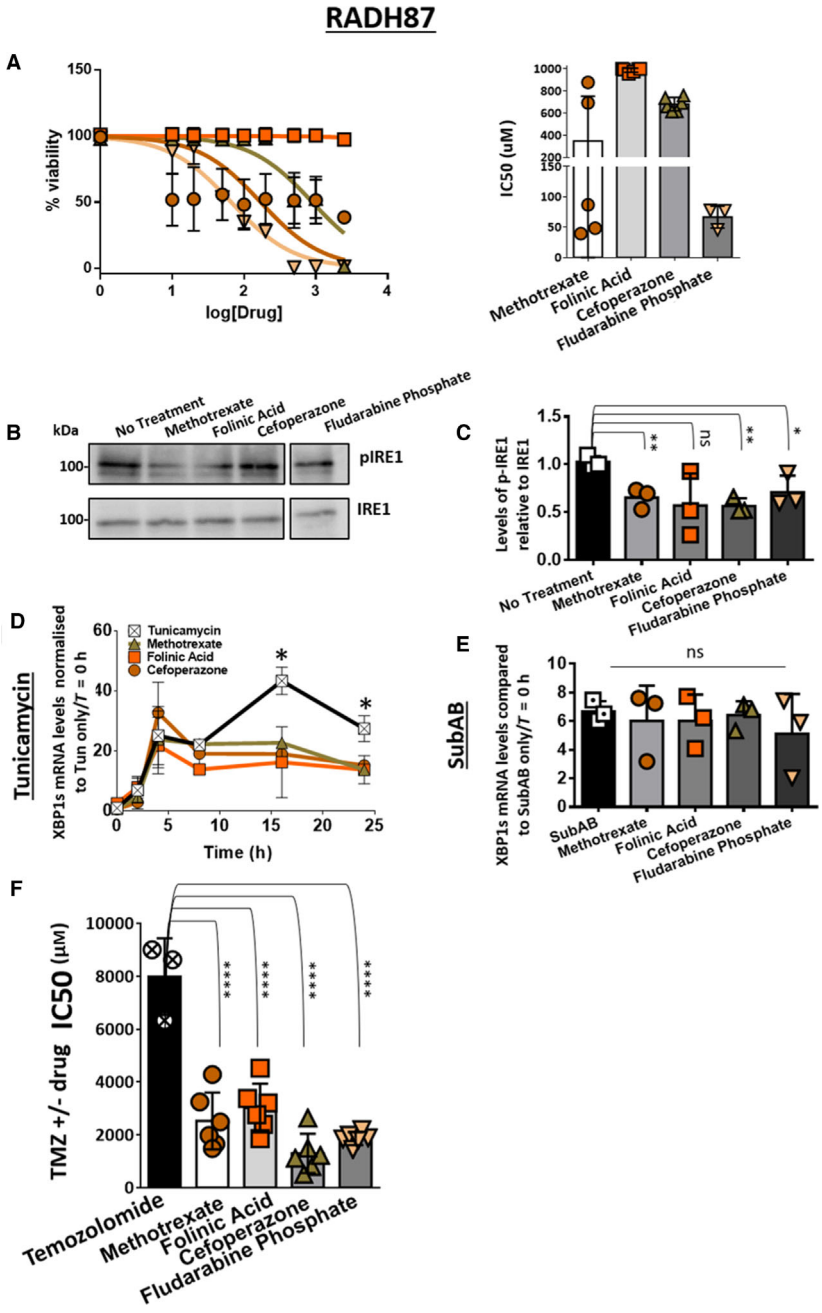

and F6P2 were synthesised and purchased from Biomatik (Cambridge, Canada). Methotrexate, folinic acid and cefoperazone were from Apollo Scientific (Stockport, UK), and fludarabine phosphate was from Selleck Chemicals (Munich, Germany).

IRE1-mediated in vitro RNase assay

Peptides were diluted in reaction buffer, organic molecules in minimal volume of DMSO, and subsequently rediluted in reaction buffer. Maximum volume of DMSO per reaction never exceeded 1%. Reaction volume was 25 μL. Recombinant IRE1 (200 μM) was incubated at room temperature for 10 min with varying concentrations (0–50 μM) of inhibitor and reaction buffer. Subsequently, equal volume of mixture of reaction buffer, ATP (1 mM), DTT (1 mM) and fluorescent probe was added to each sample and fluorescence was read in a 96-well, black, flat-bottom plate every minute for 25 min, at 37 °C, in a Tecan 200 plate reader (Tecan Group Ltd, Männedorf, Switzerland).

17424658, 2021, 3, Downloaded from https://febs.onlinelibrary.wiley.com/doi/10.1111/febs.15372 by Universite de Rennes, Wiley Online Library on [23/01/2023]. See the Terms and Conditions (https://onlinelibrary.wiley.com/terms-and-conditions) on Wiley Online Library for rules of use; OA articles are governed by the applicable Creative Commons License

Fig. 6. FDA-approved drugs predicted to bind the IRE1 kinase domain *in silico*, affect IRE1 activity *in vitro* and sensitise primary patient-derived GBM cellular models to TMZ. (A) Toxicity IC50s for each of the four inhibitors in RADH87 cells. Results are shown as mean ± SD ($n = 3$). Compounds not showing toxicity (flat curves) are capped to IC50s of 1000 μM. (B) Representative blot of RADH87 cell treatment, respectively, blotted for IRE1 and phospo-IRE1. $N = 3$ separate biological repeats were carried out, quantification of which can be seen in C. (C) Protein levels of IRE1 and phospho-IRE1 in RADH87 cells treated with methotrexate, folinic acid, cefoperazone and fludarabine phosphate over 24 h. Fold change in protein expression between IRE1 and phospho-IRE1 is represented in bar chart form normalised to the corresponding untreated cells. Results are shown as mean ± SD ($n = 3$). Unpaired *t*-tests were performed to test for statistical significance between each condition and untreated. $^{**}P = 0.0064$ (methotrexate), $^{**}P = 0.0014$ (cefoperazone), $^{*}P = 0.0407$ (fludarabine phosphate). (D) XBP1s mRNA levels upon treatment with 1 $\mu g \cdot mL^{-1}$ tunicamycin over 24 h normalised to untreated RADH87 cells. Results are shown as mean ± SD ($n = 3$). Multiple *t*-tests were performed to test for statistical significance between each condition and control; $^{*}P = 0.0240$ 16 h, $^{*}P = 0.0499$ 24 h. (E) XBP1s mRNA levels upon treatment with 0.5 $\mu g \cdot mL^{-1}$ SubAB toxin after 1.5 h normalised to untreated RADH87 cells. Results are shown as mean ± SD ($n = 3$). An ordinary one-way ANOVA was performed to check for statistical significance with the addition of Dunnett's multiple comparison test comparing all individual clusters to control. No statistical significance seen; (F) TMZ IC50s in the presence of nontoxic doses of IRE1 inhibitors in RADH87 cells. Results are shown as mean ± SD ($n = 6$). An ordinary one-way ANOVA was performed to check for statistical significance with the addition of Dunnett's multiple comparison test comparing all individual clusters to control. Significance summary based on 95% CL of diff.: **** = 3825–7101 methotrexate; **** = 3331–6607 folinic acid; **** = 5051–8327 cefoperazone; **** = 4491–7767 fludarabine phosphate.

Table 2. Concentrations of FDA-approved drugs in different assays. Concentrations of each inhibitor (methotrexate, folinic acid, cefoperazone and fludarabine phosphate) used in each cell line (U87 and RADH87) for each separate investigation (tunicamycin treatment, TMZ sensitisation, protein extraction).

	U87			RADH87		
	Concentration (μM)			Concentration (μM)		
Compound	24-h tunicamycin treatment	TMZ sensitisation assay	24-h inhibitor treatment for protein extraction	24-h tunicamycin treatment	TMZ sensitisation assay	24-h inhibitor treatment for protein extraction
Methotrexate	50	100	50	50	50	50
Folinic acid	50	100	50	50	100	50
Cefoperazone	50	100	50	50	50	50
Fludarabine phosphate	5	5	5	5	5	5

Cell culture and treatments

U87MG (ATCC) cells were authenticated as recommended by AACR (http://aacrjournals.org/content/cell-line-authentication-information) and tested for the absence of mycoplasma using MycoAlert® (Lonza, Basel, Switzerland) or MycoFluor (Invitrogen, Carlsbad, CA, USA). U87MG cells were grown in DMEM GlutaMAX (Invitrogen) supplemented with 10% FBS. Primary GBM RADH87 cells were generated as previously described [28]. For XBP1s induction experiments, tunicamycin was used at 1 $\mu g \cdot mL^{-1}$ for the indicated periods of time. SubAB toxin was used at 1 $\mu g \cdot mL^{-1}$ up to 1.5 h. Inhibitors investigated were used at subtoxic concentrations indicated in Table 2. For inhibitor cell toxicity (Fig. 6), assays cells were plated in 96-well plates at 5000 cells per well and treated with 0, 5, 10, 25, 50, 100, 250, 500, 1000 and 2500 μM concentrations of each inhibitor. After 6 days of incubation, WST1 reagent (Roche, Basel, Switzerland) was added to each well, and after 4-h incubation, the plate was read using a Tecan 200 colorimeter (Tecan Group Ltd). For TMZ sensitivity assays, cells were plated in a 96-well plate at 5000 cells per well and co-treated with 0, 5, 10, 25, 50, 100, 250, 500, 1000 and 2500 μM of TMZ plus a nontoxic dose of inhibitor described in Table 2. After 6 days of incubation, WST1 reagent (Roche) was added to each well, and after 4-h incubation, the plate was read using a Tecan 200 colorimeter. Peptides F6P1 and F6P2 were transfected in HEK293T cells using Pro-Ject™ Protein Transfection Reagent Kit (Thermo Fisher Scientific, Waltham, MA, USA) according to the manufacturer's instructions.

Statistical analyses

Data are presented as mean ± SD. Statistical significance ($P < 0.05$ or less) was determined using unpaired *t*-tests or ANOVA as appropriate and performed using GRAPHPAD PRISM software (GraphPad Software, San Diego, CA, USA). Toxicity and sensitisation curve extrapolation was performed using curve fit hypotheses by GRAPHPAD PRISM software (GraphPad Software).

17424658, 2021, 3, Downloaded from https://febs.onlinelibrary.wiley.com/doi/10.1111/febs.15372 by Universite de Rennes, Wiley Online Library on [23/01/2023]. See the Terms and Conditions (https://onlinelibrary.wiley.com/terms-and-conditions) on Wiley Online Library for rules of use; OA articles are governed by the applicable Creative Commons License

Pharmacophore generation and virtual screening

Libraries of compounds were formed using Maestro Suites 2015-2018 (Schrödinger Release 2018-4: Schrödinger, LLC, New York, NY, USA 2018) and specifically utilising tools within this program such as LigPrep, Glide Dock, Pharmacophore Hypothesis Generation, Glide grid generation and Protein preparation. Structural exploration and peptide modifications were carried out using software SuperMimic [38] and MOE (MOE 2018.01: Chemical computing group, Montreal Canada), respectively. UCSF Chimera [39] was used for image generation. Pharmacophore hypotheses were tested against a database of FDA-approved drugs using the supercomputer cluster Hebbe at the C3SE supercomputing centre (Gothenburg, Sweden), which was also utilised for all docking experiments. In the ligand preparation, all stereoisomers and tautomers were generated. As an effect, the optimal peptides and their resulting pharmacophores in some cases are based on a mix of D- and L-amino acids.

Quantitative real-time PCR

Total RNA was prepared using the TRIzol reagent (Invitrogen). All RNAs were reverse-transcribed with maxima reverse transcriptase (Thermo Scientific, Waltham, MA, USA), according to manufacturer protocol. qPCR was performed via a StepOnePlus™ Real-Time PCR Systems from Applied Biosystems (Foster City, CA, USA) and the SYBR Green PCR Core Reagents Kit (Takara, Saint-Germain-en-Laye, France). Analysis was carried out using QuantStudio™ Design and Analysis software version 1.3.1. Three technical repeats were performed per experiment. At least three biological repeats were performed per point per experiment. The primers used were as previously described [40].

Western blotting analyses

All IRE1 signalling analyses were carried out as described previously [31]. Cells grown on 6-well plates were washed with PBS and lysed with RIPA lysis buffer at 4°C for 25 min to extract protein. Cell extracts were resolved by SDS/PAGE and transferred to PVDF membranes. The resulting membranes were incubated with primary antibodies for 16 h at 4 °C, washed with PBS and incubated for 1 h with goat anti-rabbit secondary antibodies at room temperature (Invitrogen) prior revelation using chemiluminescence. The antibodies used were as previously described [40].

Microscale thermophoresis (MST)

The direct binding of the peptides F6P1 and F6P2 to IRE1 protein was measured using MST. IRE1 wild-type recombinant protein encoding the cytoplasmic domain (amino acids 465–977) with N-terminal polyhistidine-tag and GST tag (Sino Biological Europe GmbH, Eschborn, Germany, #11905-H20B) was labelled using RED-Tris-NTA fluorescent dye (RED-Tris-NTA 2nd Generation, NanoTemper, Munich, Germany; # MO-L018). For the labelling step, 100 μL of 20 nM protein solution is mixed with 100 μL of 10 nM RED-Tris-NTA dye in PBST buffer (PBS with 0.05% Tween-20) and incubated for 30 min at RT. The protein–dye mixture was centrifuged for 10 min at 4 °C and 15 000 ***g***. For measurement of direct binding, the peptides were analysed in a 16-point dilution series mixed in a 1 : 1 ratio with the labelled protein in MST buffer (50 mM Tris/HCl pH 7.8, 150 mM NaCl, 10 mM $MgCl_2$, 0.05% Tween-20). The assay was performed in standard Monolith NT.115 Capillaries (NanoTemper; #MO-K022), and all measurements were performed at 60% MST power and 40% excitation power using the Monolith NT.115Pico machine (NanoTemper). The dissociation constant (K_d) was calculated by taking the average of triplicate normalised fluorescence data (Fnorm) using NANOTEMPER analysis software (MO.Affinity Analysis v2.3). Fnorm values were converted to fraction-bound data, and the resulting binding curves are plotted using GRAPHPAD PRISM software (GraphPad Software).

Acknowledgements

This work was supported by grants from Institut National du Cancer (INCa; PLBIO), Agence Nationale de la Recherche (ANR in the framework of ERA-NET; ERAAT) and Fondation pour la Recherche Médicale (FRM; Equipe labellisée 2018) to EC. DD, AC, CC, AS, LAE and EC are funded by EU H2020 MSCA ITN-675448 (TRAINERS) and MSCA RISE-734749 (INSPIRED) grants. The Swedish Research Council (VR) and the Swedish National Infrastructure for Computing (SNIC) are gratefully acknowledged for funding and allocations of computing time at the C3SE ('Hebbe') supercomputing centre (LAE). MST measurements (CC) were performed at 2bind GmbH, Germany. We thank Dr. Thomas Schubert for support with MST analysis.

Conflict of interest

AS, EC and LAE are founders of Cell Stress Discoveries Ltd. The authors declare no conflicting interests.

Author contributions

DD, EC, AC and LAE designed the study. DD and AC performed all calculations. DD and CC performed all assays. DD and AC wrote the first draft. All authors revised the text.

17424658, 2021, 3, Downloaded from https://febs.onlinelibrary.wiley.com/doi/10.1111/febs.15372 by Universite de Rennes, Wiley Online Library on [23/01/2023]. See the Terms and Conditions (https://onlinelibrary.wiley.com/terms-and-conditions) on Wiley Online Library for rules of use; OA articles are governed by the applicable Creative Commons License

References

1 Almanza A, Carlesso A, Chintha C, Creedican S, Doultsinos D, Leuzzi B, Luís A, McCarthy N, Montibeller L, More S *et al.* (2019) Endoplasmic reticulum stress signalling – from basic mechanisms to clinical applications. *FEBS J* **286**, 241–278.

2 Doultsinos D, Avril T, Lhomond S, Dejeans N, Guédat P & Chevet E (2017) Control of the unfolded protein response in health and disease. *SLAS Discov Adv Life Sci R&D* **22**, 787–800.

3 Lhomond S, Avril T, Dejeans N, Voutetakis K, Doultsinos D, McMahon M, Pineau R, Obacz J, Papadodima O, Jouan F *et al.* (2018) Dual IRE1 RNase functions dictate glioblastoma development. *EMBO Mol Med* **10**, e7929.

4 Ming J, Ruan S, Wang M, Ye D, Fan N, Meng Q, Tian B & Huang T (2015) A novel chemical, STF-083010, reverses tamoxifen-related drug resistance in breast cancer by inhibiting IRE1/XBP1. *Oncotarget* **6**, 40692–40703.

5 Sheng X, Arnoldussen YJ, Storm M, Tesikova M, Nenseth HZ, Zhao S, Fazli L, Rennie P, Risberg B, Wæhre H *et al.* (2015) Divergent androgen regulation of unfolded protein response pathways drives prostate cancer. *EMBO Mol Med* **7**, 788–801.

6 Chien W, Ding LW, Sun QY, Torres-Fernandez LA, Tan SZ, Xiao J, Lim SL, Garg M, Lee KL, Kitajima S *et al.* (2014) Selective inhibition of unfolded protein response induces apoptosis in pancreatic cancer cells. *Oncotarget* **5**, 4881–4894.

7 Logue SE, McGrath EP, Cleary P, Greene S, Mnich K, Almanza A, Chevet E, Dwyer RM, Oommen A, Legembre P *et al.* (2018) Inhibition of IRE1 RNase activity modulates the tumor cell secretome and enhances response to chemotherapy. *Nat Commun* **9**, 3267.

8 Le Reste JP, Pineau R, Samal J, Jégou G, Lhomond S, Gorman AM, Samali A, Patterson JB, Zeng Q, Pandit A *et al.* (2019) Development of a novel preclinical glioblastoma mouse model and therapeutic impact of IRE1 inhibition. *bioRxiv* 841296. https://doi.org/10.1101/841296

9 Zhao N, Cao J, Xu L, Tang Q, Dobrolecki LE, Lv X, Talukdar M, Lu Y, Wang X, Hu DZ *et al.* (2018) Pharmacological targeting of MYC-regulated IRE1/XBP1 pathway suppresses MYC-driven breast cancer. *J Clin Invest* **128**, 1283–1299.

10 Hetz C, Chevet E & Harding HP (2013) Targeting the unfolded protein response in disease. *Nat Rev Drug Discov* **12**, 703–719.

11 Wang L, Perera BGK, Hari SB, Bhhatarai B, Backes BJ, Seeliger MA, Schürer SC, Oakes SA, Papa FR & Maly DJ (2012) Divergent allosteric control of the IRE1α endoribonuclease using kinase inhibitors. *Nat Chem Biol* **8**, 982–989.

12 Feldman HC, Tong M, Wang L, Meza-Acevedo R, Gobillot TA, Lebedev I, Gliedt MJ, Hari SB, Mitra AK, Backes BJ *et al.* (2016) Structural and functional analysis of the allosteric inhibition of IRE1α with ATP-competitive ligands. *ACS Chem Biol* **11**, 2195–2205.

13 Bouchecareilh M, Higa A, Fribourg S, Moenner M & Chevet E (2011) Peptides derived from the bifunctional kinase/RNase enzyme IRE1α modulate IRE1α activity and protect cells from endoplasmic reticulum stress. *FASEB J* **25**, 3115–3129.

14 Bouchecareilh M, Caruso M-E, Roby P, Parent S, Rouleau N, Taouji S, Pluquet O, Bosse R, Moenner M & Chevet E (2010) AlphaScreen-based characterization of the bifunctional kinase/RNase IRE1α: a novel and atypical drug target. *J Biomol Screen* **15**, 406–417.

15 Halgren TA, Murphy RB, Friesner RA, Beard HS, Frye LL, Pollard WT, & Banks JL (2004) Glide: a new approach for rapid, accurate docking and scoring. 2. Enrichment factors in database screening. *J Med Chem* **47**, 1750–1759.

16 Ali MM, Bagratuni T, Davenport EL, Nowak PR, Silva-Santisteban MC, Hardcastle A, McAndrews C, Rowlands MG, Morgan GJ, Aherne W *et al.* (2011) Structure of the Ire1 autophosphorylation complex and implications for the unfolded protein response. *EMBO J* **30**, 894–905.

17 Harrington PE, Biswas K, Malwitz D, Tasker AS, Mohr C, Andrews KL *et al.* (2014) Unfolded protein response in cancer: IRE1α inhibition by selective kinase ligands does not impair tumor cell viability. *ACS Med Chem Lett* **6**, 68–72.

18 Sterling T & Irwin JJ (2015) ZINC 15–ligand discovery for everyone. *J Chem Inf Model* **55**, 2324–2337.

19 Friesner RA, Murphy RB, Repasky MP, Frye LL, Greenwood JR, Halgren TA, Sanschagrin PC & Mainz DT (2006) Extra precision glide: docking and scoring incorporating a model of hydrophobic enclosure for protein−ligand complexes. *J Med Chem* **49**, 6177–6196.

20 Jorgensen WL & Tirado-Rives J (1988) The OPLS force field for proteins. Energy minimizations for crystals of cyclic peptides and crambin. *J Am Chem Soc* **110**, 1657–1666.

21 Farber S, Diamond LK, Mercer RD, Sylvester RF & Wolff JA (1948) Temporary remissions in acute leukemia in children produced by folic acid antagonist, 4-aminopteroyl-glutamic acid (aminopterin). *N Engl J Med* **238**, 787–793.

22 Cutolo M, Sulli A, Pizzorni C, Seriolo B & Straub RH (2001) Anti-inflammatory mechanisms of methotrexate in rheumatoid arthritis. *Ann Rheum Dis* **60**, 729–735.

23 Shiroky JB, Neville C, Esdaile JM, Choquette D, Zummer M, Hazeltine M, Bykerk V, Kanji M, St-Pierre A, Robidoux L & *et al.* (2018) Low-dose methotrexate with leucovorin (folinic acid) in the management of rheumatoid arthritis. Results of a multicenter

17424658, 2021, 3, Downloaded from https://febs.onlinelibrary.wiley.com/doi/10.1111/febs.15372 by Universite de Rennes, Wiley Online Library on [23/01/2023]. See the Terms and Conditions (https://onlinelibrary.wiley.com/terms-and-conditions) on Wiley Online Library for rules of use; OA articles are governed by the applicable Creative Commons License

randomized, double-blind, placebo-controlled trial. *Arthritis Rheum* **36**, 795–803.
24 Jones RN & Barry AL (1983) Cefoperazone: a review of its antimicrobial spectrum, β-lactamase stability, enzyme inhibition, and other in vitro characteristics. *Rev Infect Dis* **5**, S108–S126.
25 Keating MJ, Kantarjian H, Talpaz M, Redman J, Koller C, Barlogie B, Velasquez W, Plunkett W, Freireich EJ & McCredie KB (1989) Fludarabine: a new agent with major activity against chronic lymphocytic leukemia. *Blood* **74**, 19–25.
26 Carlesso A, Chintha C, Gorman AM, Samali A & Eriksson LA (2019) Effect of kinase inhibiting RNase attenuator (KIRA) compounds on the formation of face-to-face dimers of inositol-requiring enzyme 1: insights from computational modeling. *Int J Mol Sci* **6**, 1–14.
27 Wiseman RL, Zhang Y, Lee KPK, Harding HP, Haynes CM, Price J, Sicheri F & Ron D (2010) Flavonol activation defines an unanticipated ligand-binding site in the kinase-RNase domain of IRE1. *Mol Cell* **38**, 291–304.
28 Avril T, Etcheverry A, Pineau R, Obacz J, Jegou G, Jouan F, Le Reste P-J, Hatami M, Colen RR, Carlson BL *et al.* (2017) CD90 expression controls migration and predicts dasatinib response in glioblastoma. *Clin Cancer Res* **23**, 7360–7374.
29 Wolfson JJ, May KL, Thorpe CM, Jandhyala DM, Paton JC & Paton AW (2008) Subtilase cytotoxin activates PERK, IRE1 and ATF6 endoplasmic reticulum stress-signalling pathways. *Cell Microbiol* **10**, 1775–1786.
30 Paton AW, Beddoe T, Thorpe CM, Whisstock JC, Wilce MCJ, Rossjohn J, Talbot UM & Paton JC (2006) AB_5 subtilase cytotoxin inactivates the endoplasmic reticulum chaperone BiP. *Nature* **443**, 548–552.
31 Bertolotti A, Zhang Y, Hendershot LM, Harding HP & Ron D (2000) Dynamic interaction of BiP and ER stress transducers in the unfolded-protein response. *Nat Cell Biol* **2**, 326–332.
32 Byres E, Paton AW, Paton JC, Löfling JC, Smith DF, Wilce MCJ, Talbot UM, Chong DC, Yu H, Huang S *et al.* (2008) Incorporation of a non-human glycan mediates human susceptibility to a bacterial toxin. *Nature* **456**, 648–652.
33 WHO | WHO Model Lists of Essential Medicines (2018) World Health Organization. Available from: http://www.who.int/medicines/publications/essentialmedicines/en/.
34 Gibson EM, Nagaraja S, Ocampo A, Tam LT, Wood LS, Pallegar PN, Greene JJ, Geraghty AC, Goldstein AK, Ni L *et al.* (2019) Methotrexate chemotherapy induces persistent tri-glial dysregulation that underlies chemotherapy-related cognitive impairment. *Cell* **176**, 43–55.
35 Cross BCS, Bond PJ, Sadowski PG, Jha BK, Zak J, Goodman JM, Silverman RH, Neubert TA, Baxendale IR, Ron D & *et al.* (2012) The molecular basis for selective inhibition of unconventional mRNA splicing by an IRE1-binding small molecule. *Proc Natl Acad Sci USA* **109**, E869–E878.
36 Sanches M, Duffy NM, Talukdar M, Thevakumaran N, Chiovitti D, Canny MD, Lee K, Kurinov I, Uehling D, Al-awar R *et al.* (2014) Structure and mechanism of action of the hydroxy–aryl–aldehyde class of IRE1 endoribonuclease inhibitors. *Nat Commun* **5**, 4202.
37 Paton AW, Srimanote P, Talbot UM, Wang H & Paton JC (2004) A new family of potent AB_5 cytotoxins produced by Shiga toxigenic *Escherichia coli*. *J Exp Med* **200**, 35–46.
38 Goede A, Michalsky E, Schmidt U & Preissner R (2006) SuperMimic–fitting peptide mimetics into protein structures. *BMC Bioinformatics* **7**, 11.
39 Pettersen EF, Goddard TD, Huang CC, Couch GS, Greenblatt DM, Meng EC & Ferrin TE (2004) UCSF Chimera – a visualization system for exploratory research and analysis. *J Comput Chem* **25**, 1605–1612.
40 Sicari D, Delaunay-Moisan A, Combettes L, Chevet E & Igbaria A (2019) A guide to assessing endoplasmic reticulum homeostasis and stress in mammalian systems. *FEBS J* **287**, 27–42.

17424658, 2021, 3, Downloaded from https://febs.onlinelibrary.wiley.com/doi/10.1111/febs.15372 by Universite de Rennes, Wiley Online Library on [23/01/2023]. See the Terms and Conditions (https://onlinelibrary.wiley.com/terms-and-conditions) on Wiley Online Library for rules of use; OA articles are governed by the applicable Creative Commons License